49th AIAA Aerospace Sciences Meeting including the New Horizons Forum and Aerospace Exposition
4 - 7 January 2011, Orlando, Florida
AIAA 2011-1075

Study of Transient and Unsteady Effects of Plasma Actuation in Transitional Flow over an SD7003 Airfoil

Mark Riherd[1] and Subrata Roy[2]
Applied Physics Research Group, Dept. of Mechanical and Aerospace Engineering, University of Florida, Gainesville, FL, 32054

Don Rizzetta[3] and Miguel Visbal[4]
Computational Sciences Branch, Air Vehicles Directorate, Air Force Research Laboratory, Wright Patterson Air Force Base, OH 45433

The short term transient and long term periodic unsteady effects of pulsed plasma actuation are studied using an unsteady, compressible Navier-Stokes solver for the case of a partially separated transitional flow over an SD7003 airfoil at 4° angle of attack and at Re=40,000. Forcing magnitude and its effect on the flow field is examined. Distinctly different behavior is observed parameters are adjusted. The unsteady simulations show that the actuators have a quick transient response, reattaching the separated flow within 2 nondimensionalized units of time, but nearly independently of the forcing magnitude. Spikes in C_l, C_d, and C_m are observed during reattachment, most likely due to vortex pairing at the trailing edge.

Nomenclature

c	=	Chord length
C_d	=	Coefficient of drag
C_f	=	Coefficient of skin friction
C_l	=	Coefficient of lift
C_m	=	Coefficient of moment
C_p	=	Coefficient of pressure
D_c	=	Nondimensional plasma force magnitude
E	=	Energy
E_c	=	Characteristic electrical field
e_c	=	Electron charge
ξ, ζ, η	=	Body fitted coordinates
f_i	=	Body force in the i direction
St	=	Nondimensional forcing
F, **G**, **H**	=	Inviscid flux vectors
$\mathbf{F_v}$, $\mathbf{G_v}$, $\mathbf{H_v}$	=	Viscid flux vectors
γ	=	Ratio of specific heats
$\mathcal{J}$	=	Jacobian
M	=	Mach number
p	=	Pressure
ρ	=	Density
ρ_c	=	Characteristic electron density
Q_i	=	Heat Flux
Q	=	Vector of dependent flow variables

[1] Graduate Research Assistant, Student Member AIAA
[2] Associate Professor, AIAA Associate Fellow
[3] Senior Research Aerospace Engineer, Computational Sciences Branch, AFRL/RBAC, Associate Fellow AIAA
[4] Technical Area Leader, Computational Sciences Branch, AFRL/RBAC, Associate Fellow AIAA

U, V, W	=	Contravariant velocity components
u, v, w	=	Velocity in the Cartesian coordinate system
Re	=	Reynolds number
$\boldsymbol{S}$	=	Source term vector
St	=	Strouhal number
τ	=	Nondimensional time
τ_{ij}	=	Shear stress
x,y, z	=	Cartesian coordinates

Subscripts

$_\infty$	=	Freestream reference velocity
$_{xi}$	=	Partial derivatives with respect to the xi^{th} direction

I. Introduction

THE problem of flow separation and methods to reattach flow is one of the more highly documented problems in fluid dynamics. However, a majority of the literature regarding flow reattachment in existence focuses on the long term effects determining whether the flow is still separated or if the given method is successful.

As the interest in MAVs continues to increase, the importance of understanding flow control for lower Reynolds number flow also becomes more a more important. Much work has gone into studying the equilibrium effects of flow control, airfoil design, and the general properties of flow around airfoils at these lower Reynolds numbers. Even so, the short term transient and detailed unsteady effects are not as widely documented, though material does exist ([1, 2, 3]). For MAV applications, these time dependent effects of flow control become very important, as oscillations and spikes in the non-dimensional forces C_l, C_d, and C_m can cause pitching and plunging.

The effects of Dielectric Barrier Discharge (DBD) plasma actuation as a flow control device have also been widely studied over the past decade [4], particularly for the use of flow reattachment [5, 6, 7, 8]. These actuators have a number of valuable properties as they can be flush mounted to an surface, have a near-instantaneous response, and can be pulsed at any frequency up to the 10s of kilohertz (the frequency range required to operate and Alternating Current (AC) DBD plasma actuation), even while being duty cycled at a lower frequency more characteristic of the flow. The equilibrium effects of plasma actuation in the laminar, transitional [9, 10, 11], and turbulent [11] flow regimes have all been studied.

DBD plasma actuation has been experimentally examined for a number of flow control applications, ranging from the control of entire aircraft, replacing moving control surfaces [12, 13], to turbine blade reattachment [14, 15], to aeroacoustic applications [16], and even for improved film cooling effectiveness [17]. As plasma actuation becomes more and more well understood, its potential for use with micro air vehicles (MAVs) becomes clearer, where the instantaneous level of control that plasma actuation offers is very important.

In the case studied here, a laminar separation bubble is found to exist over the suction surface of an SD7003 airfoil at a Reynolds number of 40,000 and a 4^o angle of attack. This separation bubble is common in many MAV scenarios, and its existence detrimental to airfoil performance. Beyond this bubble, the flow is found to be transitional. Plasma actuation has been shown to reattach this flow in the time-mean sense [18] by exciting an unstable frequency in the shear layer. A more similar methodology is also shown to reattach the flow using slot flow near the leading edge in [19, 20].

The focus of this study revolves around the transient effects of the flow as plasma actuation is used to reattach the flow and the unsteady effects that exist once the flow has reached an equilibrium state. While many studies referenced here have examined the reattached flow once it has reached a steady state, a majority of those studies have focused on the time mean properties, neglecting any unsteady effects that may exist. In particular this study builds on the work done by Rizzetta and Visbal [18], presenting additional results while varying the parameter D_c, and expanding upon the physical explanation presented there, particularly the unsteady effects.

II. Governing Equations and Numerical Models and Methods

This study was performed using the Implicit Large Eddy Simulation (ILES) method [21] using the implicit Beam and Warming algorithm [22] for time integration. The unsteady, three dimensional, compressible, unfiltered form of the Navier-Stokes equations is solved. The equations are solved in a generalized body-fitted coordinate system. The equations are solved in the conservation form, where

$$\frac{\partial}{\partial t}\left(\frac{1}{\mathcal{J}}\mathbf{Q}\right)+\frac{\partial}{\partial \xi}\left(\boldsymbol{F}-\frac{1}{Re}\boldsymbol{F_v}\right)+\frac{\partial}{\partial \eta}\left(\boldsymbol{G}-\frac{1}{Re}\boldsymbol{G_v}\right)+\frac{\partial}{\partial \zeta}\left(\boldsymbol{H}-\frac{1}{Re}\boldsymbol{H}\right)=D_c q_c \boldsymbol{S}$$

$\boldsymbol{Q}$ is the vector of dependent variables. The terms $\boldsymbol{F}$, $\boldsymbol{G}$, and $\boldsymbol{H}$ are the inviscid flux vectors, and $\boldsymbol{F_v}$, $\boldsymbol{G_v}$, and $\boldsymbol{H_v}$ are the viscid flux vectors. Furthermore, t represents time, and ξ, η, and ζ represents the body fitted coordinate system. The plasma forcing is included via the source term $\boldsymbol{S}$, explained in more depth below. While this is an incompressible flow, because a compressible flow solver is used, a Mach number of 0.1 is used in order to minimize compressibility effects while maintaining numerical stability. These terms are defined as the dependent variables of

$$\boldsymbol{Q}=\begin{bmatrix}\rho\\ \rho u\\ \rho v\\ \rho w\\ \rho E\end{bmatrix},$$

the inviscid flux vectors are

$$\boldsymbol{F}=\frac{1}{\mathcal{J}}\begin{bmatrix}\rho U\\ \rho uU+\xi_x p\\ \rho vU+\xi_y p\\ \rho wU+\xi_z p\\ \rho EU+\xi_i u_i p\end{bmatrix},\qquad \boldsymbol{G}=\frac{1}{\mathcal{J}}\begin{bmatrix}\rho V\\ \rho uV+\eta_x p\\ \rho vV+\eta_y p\\ \rho wV+\eta_z p\\ \rho EV+\eta_i u_i p\end{bmatrix},\qquad \text{and}\qquad \boldsymbol{H}=\frac{1}{\mathcal{J}}\begin{bmatrix}\rho W\\ \rho uW+\zeta_x p\\ \rho vW+\zeta_y p\\ \rho wW+\zeta_z p\\ \rho EW+\zeta_i u_i p\end{bmatrix},$$

the viscid flux vectors are

$$\boldsymbol{F_v}=\frac{1}{\mathcal{J}}\begin{bmatrix}0\\ \xi_{x_i}\tau_{i1}\\ \xi_{x_i}\tau_{i2}\\ \xi_{x_i}\tau_{i3}\\ \xi_{x_i}\left(u_j\tau_{ij}-Q_i\right)\end{bmatrix},\qquad \boldsymbol{G_v}=\frac{1}{\mathcal{J}}\begin{bmatrix}0\\ \eta_{x_i}\tau_{i1}\\ \eta_{x_i}\tau_{i2}\\ \eta_{x_i}\tau_{i3}\\ \eta_{x_i}\left(u_j\tau_{ij}-Q_i\right)\end{bmatrix},\quad \text{and}\quad \boldsymbol{H_v}=\frac{1}{\mathcal{J}}\begin{bmatrix}0\\ \zeta_{x_i}\tau_{i1}\\ \zeta_{x_i}\tau_{i2}\\ \zeta_{x_i}\tau_{i3}\\ \zeta_{x_i}\left(u_j\tau_{ij}-Q_i\right)\end{bmatrix},$$

where

$$U=\xi_{x_i}u_i\,,\qquad V=\eta_{x_i}u_i,\qquad \text{and}\qquad W=\zeta_{x_i}u_i$$

$$E=\frac{T}{\gamma(\gamma-1)M_\infty^2}+\frac{1}{2}(u^2+v^2+w^2)$$

The variables u,v, and w represent the Cartesian velocity components. p represent the pressure. ρ represents density. T represents temperature, and finally, E represents energy. All of these variables have been nondimensionalized by their characteristic values, except for pressure, which has been nondimensionalized by the dynamic head of the characteristic variables. The length scales have all been nondimensionalized by the chord length of the airfoil.

This force is derived from the ionization of the air between two asymmetrically placed electrodes, separated by a dielectric material (Figure 1). The magnitude of this forcing is controlled by the nondimensional parameter D_c, being the ratio of twice the maximum possible plasma work to the dynamic head. The phenomenological model [23] for the plasma was used. While this model is simplest of the available models, the primary purpose of the plasma in these simulations is not an in depth study of how the flow is affected in the plasma region, but how disturbances due to plasma actuation affects the flow overall. Additionally, recent results [18] have shown that there is relative independence of the plasma model to the end result under certain conditions, similar to in this simulation. The plasma source is formally described for these simulations as

$$\boldsymbol{S}=\frac{1}{\mathcal{J}}\begin{bmatrix}0\\ f_x\\ f_y\\ f_z\\ f_i u_i\end{bmatrix}\text{ and }D_c=\frac{\rho_c q_c e_c E_c c}{\rho_\infty u_\infty^2}.$$

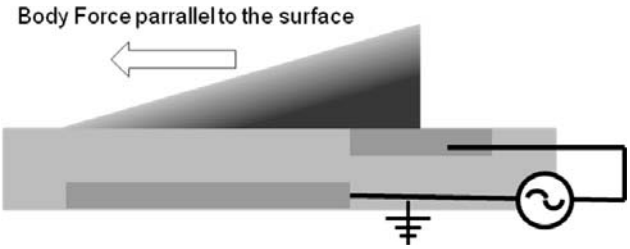

Figure 1. Diagram of a DBD plasma actuator. Two electrodes (the upper powered and the lower grounded) are asymmetrically separated by a dielectric material. During operation, the gas region from the powered to grounded electrodes is weakly ionized.

The equations shown above are the unfiltered Navier-Stokes equations. Using the Implicit Large Eddy Simulation (ILES) method, these equations are filtered through a post-processing step using Pade-type filters developed by Visbal and Gaitonde [24] based on the pentadiagonal type filtering scheme initial developed by Lele [25].

The computations for this study were done on a cylindrical O-mesh of 390x242x51 (angular x radial x spanwise) points representing an SD7003 airfoil with a unit chord length and extended 0.2 chord lengths in the spanwise direction with periodic boundary conditions applied spanwise (Figure 2). The mesh extends outwards over 100 chord lengths in order to provide a good free stream condition. The mesh is also stretched as it goes to the free stream in order to prevent reflections off of the free stream boundary.

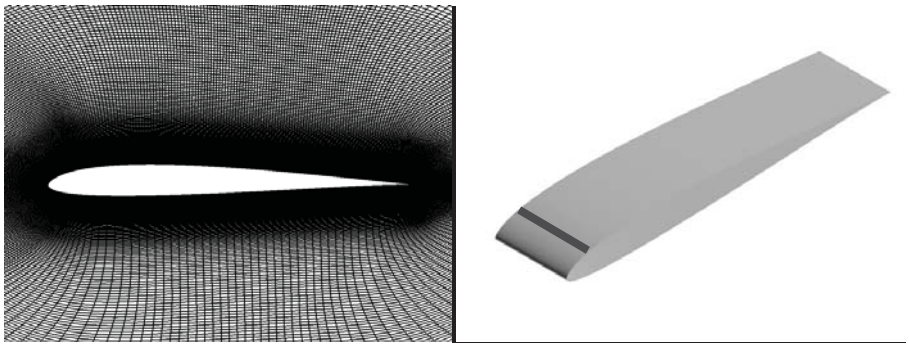

Figure 2. The computational mesh used (left) and the location of the plasma actuation (right) are shown.

After running for 100,000 (10 non dimensional units of time, τ, where $\tau=u_\infty/c$) times steps to remove any irregularities, a baseline flow for the SD7003 airfoil was established. This flow was used as an initial condition for all of the cases tested. All of the cases were run for at least 5τ in order to reach an equilibrium state where the transient effects could be considered negligible. The cases run are shown in Table 1.

Table 1. Pulsing frequency and force magnitude of the cases run.

Case	Pulsing Freq. (St)	Dc
Baseline	n/a	n/a
Steady Actuation	0.0	39.2599
2x Steady Actuation	0.0	78.5398
1/8 Force	5.0	4.9087
¼ Force	5.0	9.8175
½ Force	5.0	19.6350
Baseline Pulsed Actuation Case	5.0	39.2599
2x Force	5.0	78.5198

IV. Results

A. Baseline Case

A baseline case was run in order to reach an equilibrium solution at a Reynolds number of 40,000 and a 4º angle of attack. This solution shows a separated shear layer on the upper surface of the airfoil, which transitions about

halfway down the chord. The time averaged properties shown below have been averaged from 100 samples over a time span of 5τ.

These flow fields and turbulent kinetic energies qualitatively match up well with reported experimental and numerical results (Figure 3, 4, and 5). The instantaneous flow fields show the documented vortical shedding, as well as the separation bubble. The time averaged data shows the separation bubble, as well as the turbulizing effects once the flow reattaches near the trailing edge. See [19, 26, 27] for more detailed information about the SD7003 flow field across a range of parameters.

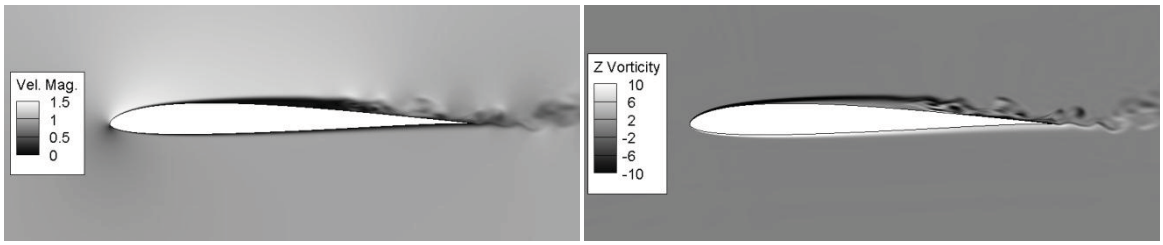

Figure 3. 2D Instantaneous velocity magnitude (left) and z-vorticity (right) at the center slice at τ=0.

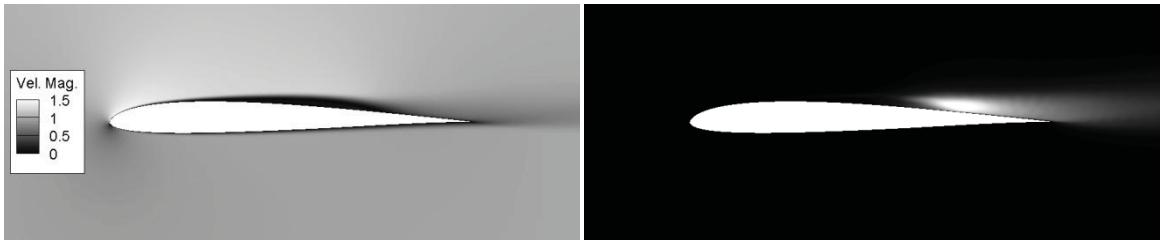

Figure 4. 2D Time and spanwise averaged velocity magnitude (right) and turbulent kinetic energy (left).

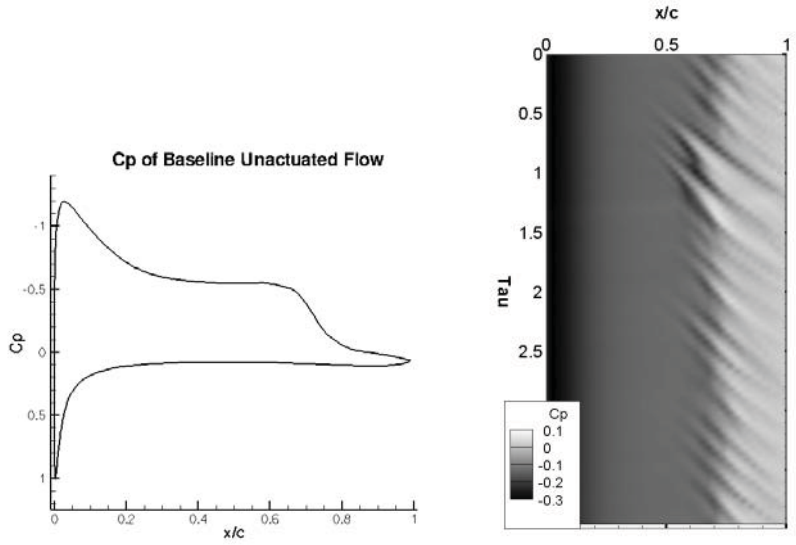

Figure 5. Time and spanwise averaged (left) and time evolving (right) upper surface pressure coefficient (starting at the initial condition shown).

The time evolving surface pressure shown above in Figure 5 shows several features that will be further dissected once the plasma control is implemented. The large grey area from the leading edge to mid-chord indicates the stable low pressure laminar separation bubble. From the mid-chord to the trailing edge, the streaky area shows the presence of a quasi-regular shedding off of the separation bubble. This shedding, while occurring at a somewhat regular frequency (approximately St=5.0) does not occur with a consistent magnitude, which causes the irregular forces experienced by the airfoil. The higher pressure region near the trailing edge indicates the region where the transition to turbulence has reattached the flow.

B. Reattachment of the Flow with Pulsed Forcing

Using plasma actuation, it is possible to reattach the partially separated transitional flow shown above. Both steady and duty-cycled plasma actuation were tested, with significant results found only with the duty-cycled actuation. While plasma actuation has been previously shown to be able to reattach separated flows using continuous actuation, at higher Reynolds numbers and lower amounts of plasma body force, this method is less effective (similar results have been seen using Vortex Generator Jets (VGJs) in use for turbine flow separation control [28]). Two cases were run with the actuators in a counter-flow configuration at D_c=39.3, and 78.6 with continuous plasma forcing. The higher value of plasma forcing showed a slight amount of flow control when it was initially activated, but these effects ultimately led to more unsteady lift, drag, and moments on the airfoil than for the baseline case with no plasma actuation.

The reattachment process explained below is for the case of the plasma forcing being equal to D_c=39.3, and the forcing frequency of St=5.0 (corresponding to an instability existing in the separation region) with a 50% duty cycle.

The flow initially has a separation bubble over the majority of the chord length on the suction side of the airfoil. The flow over the last third of the chord begins to transition and reattach itself to the airfoil while occasionally shedding vortices off of the laminar separation bubble. The reattachment of the flow takes place in several stages (Figure 6, below).

When turned on, the plasma actuator, operating in a counter flow orientation and pushing against the flow, will actually reduce the momentum in the near wall region where the body force is applied. Though the momentum in the plasma region is reduced, the actuator is actually bringing momentum closer to the surface due to shed vortical structures that increase the mixing between the freestream and separated shear layer.

In the first stage of the reattachment, disturbances caused by the plasma actuator travel through the separated shear layer and excite instabilities in this layer. Once unstable, the separated region breaks apart and becomes a number of discrete and coherent vortical structures. These vortical structures may vary in their size, spacing, and vorticity depending on the magnitude and forcing frequency (some of the details are explained layer on for other cases). This action takes place over the time τ=0.0 to τ=0.6.

Once the shear layer has broken into a number of vortical structures, these structures begin to pair up with each other. As these vortices coalesce, the size and strength of the combined vortex increases and convects downstream, it sweeps away any transitional/turbulent structures over the upper surface of the airfoil (τ=0.6 to τ=1.2).

As this large vortex passes over the trailing edge, it pairs with a counter rotating vortex. This event appears to produce the pronounced spiking effects seen in the lift, drag, and moment experienced by the airfoil and will be elaborated on further. These two vortices pair together and move downstream (τ=1.2 to τ=1.6).

This counter rotating vortex actually originates farther upstream than it appears. When each of the smaller vortical structures is created by the shear layer break up, counter rotating vortices of similar circulation are created below them due to conservation of circulations. These counter rotating vortical structures are not directly visible, but their presence does cause dips in the vorticity boundary layer, which can be seen in Figures 6 and 8. Upon reaching the trailing edge, the underlying vortex is able to escape the boundary layer, and the induced vortex pairing is finally visible.

Once the large vortical structure and its pair are sufficiently far downstream, the flow can be considered to be close to an equilibrium state. At this point, the shear layer has been regularly shedding two dimensional vortical structures due to the disturbances caused by the pulsed plasma actuator. These structures are transported downstream, slowing losing their coherence and two dimensionality, and eventually transitioning to turbulence. Should they maintain their coherence to the trailing edge, then they will induce another vortex pairing at the trailing edge, another result that will be elaborated on more later in Section IV.D.

The nondimensional forces experienced during reattachment show a very distinct, almost impulse-like behavior around the time τ=1.4 (Figure 7). Around this time, the large vortical structure created by the pairing and coalescing of the laminar separation bubble remnants is passing over the trailing edge. As this vortical structure crosses the trailing edge, it induces a second vortical structure with opposing vorticity at the trailing edge of the pressure side of the airfoil (Figure 8).

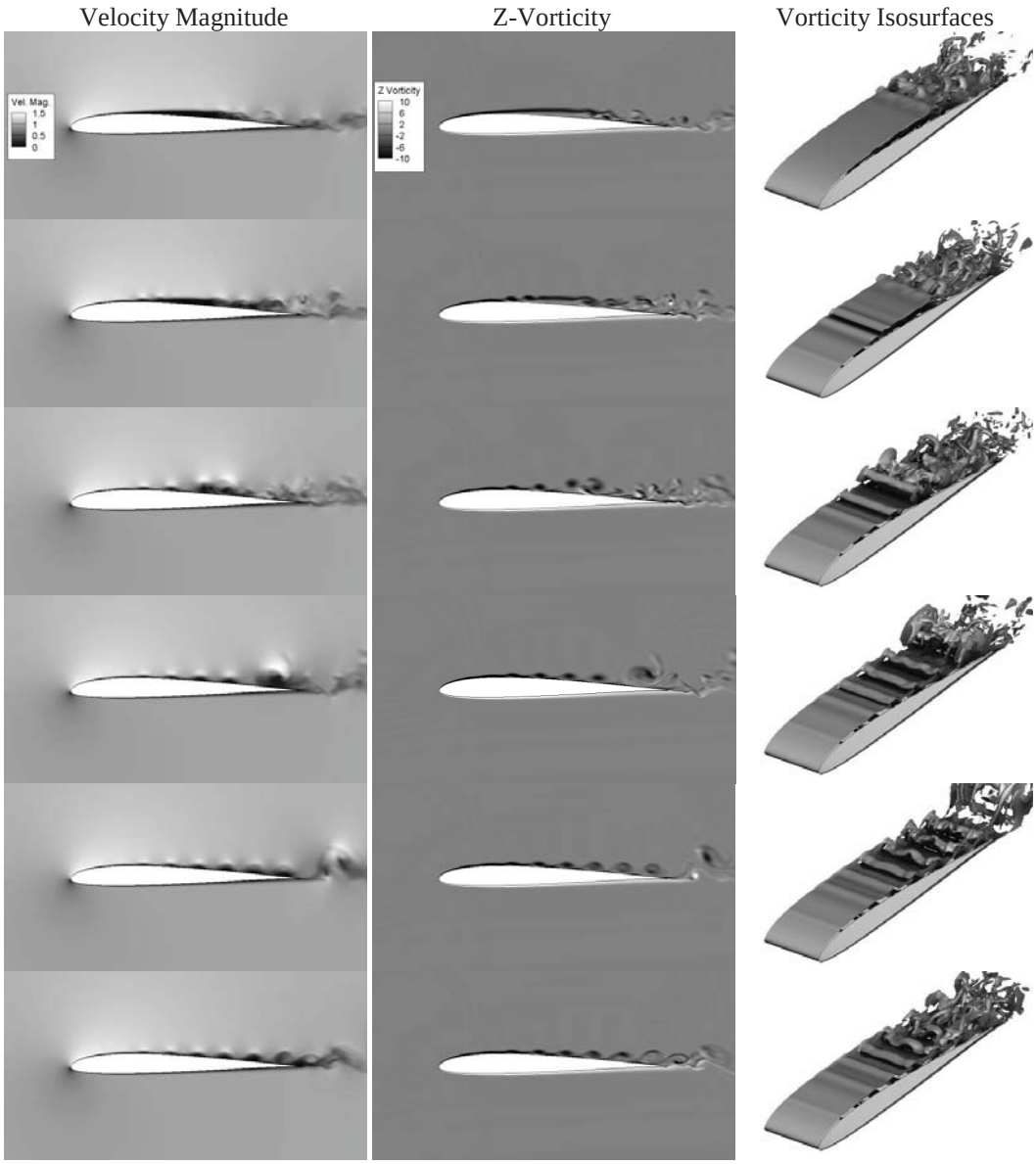

Figure 6. Instantaneous velocity magnitudes, z-vorticity and vorticity isosurfaces as the flow reattaches at τ=0.0, 0.4, 0.8, 1.2, 1.6 and 2.0 (top to bottom).

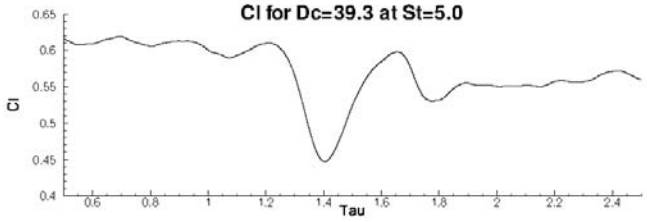

Figure 7. Transient lift on the airfoil during reattachment.

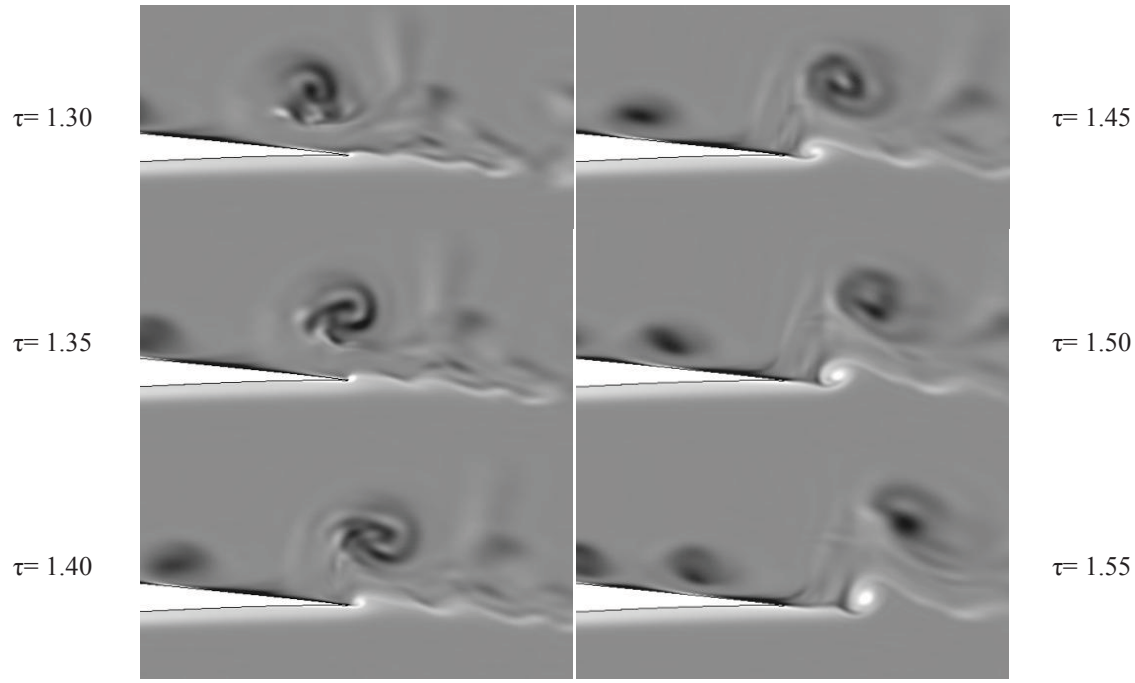

Figure 8. Z-vorticity and induce vortex pairing near the trailing edge during the induced vortical pairing from τ= 1.30 to 1.55. Smaller vortical structures shed by the plasma actuation are also present.

C. Equilibrium Unsteady Flow Effects

The long term equilibrium time averaged effects of this type of actuation under these conditions have been studied by Rizzetta and Visbal (2010) [18]. While the time averaged cases provide plenty of information about the final result in a time-mean sense, much information is lost by not studying the unsteady effects. In order to capture the appropriate physics once the flow has reached equilibrium, the properties of the flow have been phase locked as well as spanwise averaged in order to provide an accurate sampling of the flow.

In examining the flow field of the equilibrium state, it becomes immediately apparent that the vortical structures in the flow slowly lose their coherence as they move downstream, growing in size as their structure is lost (Figure 9) due to a combination of viscous effects and instabilities from their development reaching a critical magnitude. The phase locked turbulent kinetic energy further shows that the loss of coherence maintains some correlation to the transition of the flow from laminar to its transitional state (Figure 10).

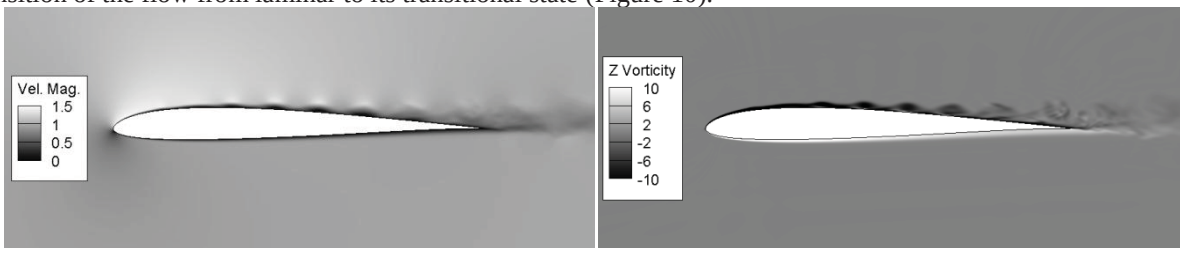

Figure 9. Phase locked (ϕ=0) and spanwise averaged velocity magnitude, z-vorticity, and turbulent kinetic energy.

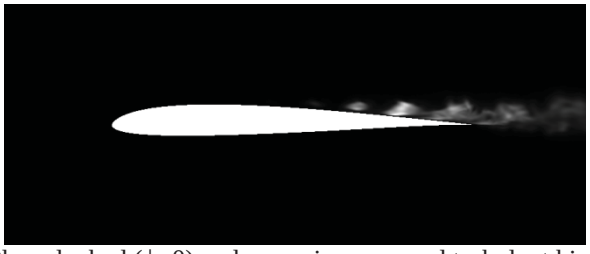

Figure 10. Phase locked (ϕ=0) and spanwise averaged turbulent kinetic energy.

The pressure on the surface of the airfoil also shows the result of these vortical structures as well. Phase averaging the surface pressure shows that the actuator creates small pressure disturbances in the shear layer. These disturbances then propagate through the shear layer, incite instabilities and cause the shear layer to shed vortices at the specified frequency (Figure 11 (left)). These vortices then travel downstream, slowly losing their coherence as they transition to turbulence. The shear stress on the surface shows a similar oscillatory behavior as well for the same reasons (Figure 11, right).

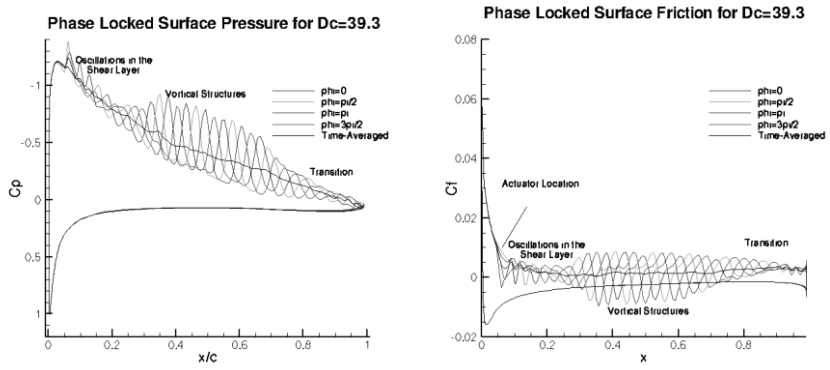

Figure 11. Phase locked surface pressure and shear stress.

D. Initial Condition Study

A previous study done by Rizzetta and Visbal (2010) [18] examined an identical flow scenario under the same effects of plasma actuation, focusing on the long term reattachment, rather than the short term reattachment process as examined here. The computational meshes used in that study were much finer, and as the equilibrium effects of that study and the present study are highly comparable, an extensive study of the grid resolution will not be presented here.

However, as the transient effects of the flow reattachment process may be dependent on the initial conditions, the effect of the initial conditions will be examined in this study. The baseline case of flow over an SD7003 airfoil was used to provide additional starting points for the initial condition study. In the case shown above, plasma actuation was started at τ=0.0 relative to the baseline case, but for this initial condition study, the plasma actuation is started at τ=1.0 and τ=2.0 in order to determine the level of dependence of reattachment to the initial conditions. These cases were only run for two nondimensional time units, which is long enough to capture the bulk of the reattachment process.

In performing this initial condition study, it was found that while small parts of the process may be dependent on the initial conditions, the major airfoil force spike is not. For all three cases (plasma started at τ=0.0, 1.0 and 2.0), the flow structure show the same large shed vortical structure and the spike in the airfoil forces is of the same magnitude and at the same time after the plasma is started (Figure 12). Smaller structures in the flow may be different due to random fluctuations in the pre-actuated transitioning process, but the large scale behavior is maintained.

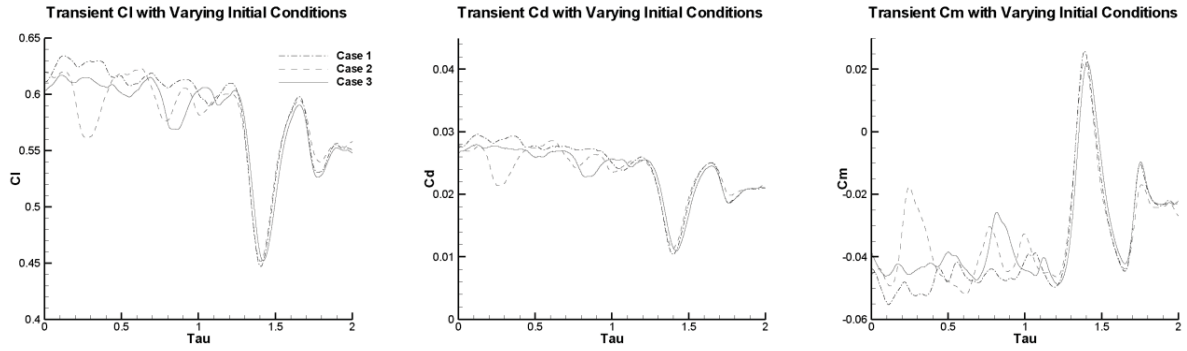

Figure 12. C_l , C_d, and C_m for the reattachment process

E. Linear Counter Flow Cases – Steady and Pulsed Forcing Magnitude Effects

As part of this study, reattachment of the flow as a function of the forcing magnitude is also studied. It was found that in reattaching the flow, that the level of plasma forcing can be very low, as long as the forcing is exciting the flow within the range of unstable frequencies. Steady actuation was found to have a slight initial effect, but even at a higher forcing magnitude (D_c=78.3), the long term effect on transitioning/reattaching the flow was negligible.

Additionally, it seems that the major transient effects associated with turning on the plasma actuation and the reattachment of the separated region (the impulse like behavior in C_l, C_d and C_m around τ=1.4) are largely independent of the forcing magnitude. Closer examination of the flow fields during reattachment show some slight changes in the way that the separation bubble wraps and the vortex pairing, but the primary mechanics of the reattachment are almost identical. As can be seen below, these spikes in force occur at the same time and cause the same level of disturbance to the nondimensional forces (Figure 13). This spike in the nondimensional forces comes at the exact time where the rolled up separation layer passes over the trailing edge. Therefore, it seems that this spike in pressure is primarily a function of the initial separation bubble and indirectly a function of the Reynolds number and angle of attack that it formed at, both of which are completely independent of the forcing magnitude. Furthermore, this suggests that the mechanism of reattachment is more highly dependent on the excitation of instabilities in the boundary layer, rather than a blunt change in momentum in low momentum separation region.

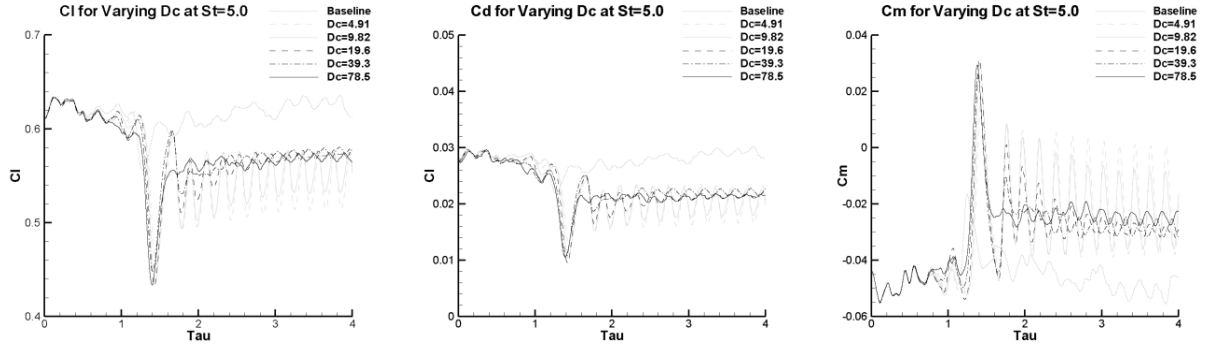

Figure 13. C_l, C_d, and C_m for increasing values of D_c.

For the D_c=39.3 case shown above, one can see the effects of the shed vortices breaking down and transitioning the flow. However, as the forcing magnitude is decreased, the oscillations of the airfoil forces (C_l, C_d, C_m) become larger. In examining the flow and surface forces, the vortical structures that are shed created remain coherent much farther downstream than for the lower magnitudes of plasma forcing.

In examining the time evolving spanwise averaged surface pressure, it becomes very clear that the reattachment process for the various forcing is almost independent of the forcing magnitudes. In Figure 14 below, the flow features examined in Section IV.B are again present. The flat grey triangular region which begins to shrink starting at tau=0.0 shows the remnants of the laminar separation bubble. The low pressure streaks indicate the presence of vortical structures. A number of these streaks are emanating from the laminar separation bubble, indicating the wrap up of the separated region into individual vortices. The most prominent feature though, the large, very low pressure streak shows the location of the large vortical structure that causes the airfoil force spike.

Further along in time, the surface pressure, just like the flow, reaches an unsteady periodic state. The loss of coherence of the vortical structures can be seen via the dissipation of the low pressure streaks. It is interesting to note that the lower forcing values produce seemingly more coherence vortical structures. It should be noted that while the vortical structures induced by the smaller disturbances (D_c=9.8) remain coherent in the wake, they do not form as quickly as those for the stronger plasma induced disturbance (D_c=39.3).

The oscillatory behavior of the nondimensional forces suggests that there is a level of control saturation at which additional forcing is not necessarily helpful around the forcing magnitude of D_c=19.6 (Figure 15, center). Time averaged lift and drag seem close to optimal at this point (Figure 15, left), and the oscillatory behavior is close to the minimum for the lift, drag and moment (Figure 15, right). At this level of forcing it seems that the vortical structures lose their coherence right before passing over the trailing edge of the airfoil. For lower values of D_c, there structures retain their coherence and only transition once they have left the airfoil surface (Figure 16). These still vortical structures that are still coherent as they leave the trailing edge of the airfoil are able to induce (though at a lower magnitude) they type of vortex pairing seen during large reattachment spike. The transition of the flow to a non-coherent transitional/turbulent state seems to be the mechanism with prevents the large scale oscillations.

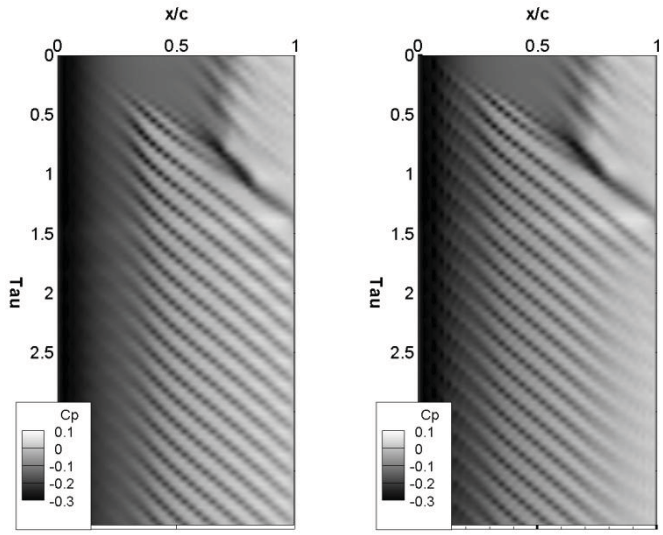

Figure 14. Time evolving spanwise averaged C_p for D_c=9.8 (left) and D_c=39.3 (right) for the suction surface.

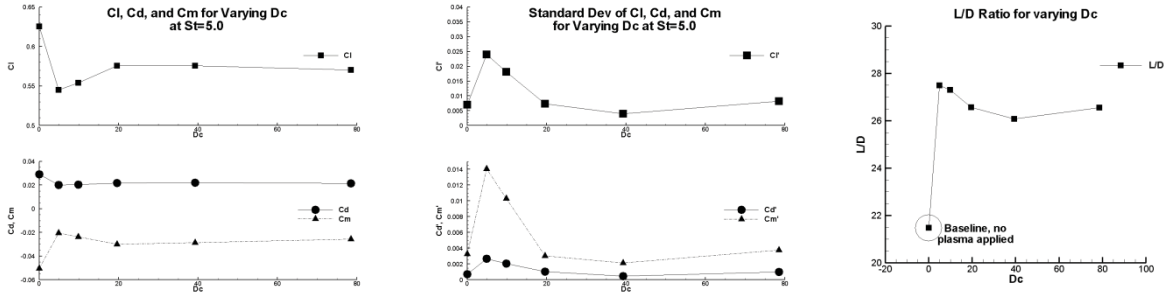

Figure 15. Equilibrium C_l, C_d, C_m, L/D, and averages and oscillations averaged from τ=3.0 to τ=5.0.

Just as with the reattachment, the induced vortex pairing at the trailing edge is again present for the lower values of plasma forcing tested (Figure 17), and now causing the large oscillatory behavior in the total forces experience by the airfoil. For these smaller vortical structures with lesser circulation, the induced vortical pairing is a smaller event than the pairing that occurs during reattachment, but still a significant feature in the equilibrium flow. This can be seen very distinctly for the cases of D_c=4.9 and D_c=9.8 in Figure 16 above as well.

Additionally, the reason for the prolonged coherence of the vortical structures and their oscillatory effect on the surface pressure for the lower magnitude forcing may be that they cause less of a disturbance in the shear layer. This smaller disturbance creates less unstable vortex shedding, and therefore longer lasting structures (Figure 18). This effect is due to the level of instability initially present when the vortical structures are shed. The plasma actuation creates the vortical structures in its operation. However, these structures appear to not be entirely stable. Thus, in their creation, should some non-uniformity in the flow alter the disturbance itself, that non-uniformity disturbs the shed vortical structures, and leads to their instability.

These results have mixed implications, both positive and negative. The positive aspects of this are that even at lower voltages, plasma actuation is effective at removing the separation bubble and increasing the lift to drag ratio. Both lift and drag decrease when plasma actuation is used, but the drag decreases significantly more than the lift, resulting in a 20% increase in the ratio of lift to drag for all cases, including the lowest tested values of plasma forcing. Opposing this increase in lift to drag is the result that the nondimensional forces acting on the airfoil become oscillatory in nature. With no actuation, the forces are random and unpredictable. For the cases of stronger actuation, the forces are stabilized, if still slightly oscillatory in nature. However, when the level of plasma forcing is decreased, the oscillations in the nondimensional forces become more significant, becoming only a single order of magnitude smaller than the overall force for lift and drag and becoming the same order of magnitude for the rotational moment coefficient. This combined unsteadiness could present itself as a very difficult pitching/plunging issue in the worst cases.

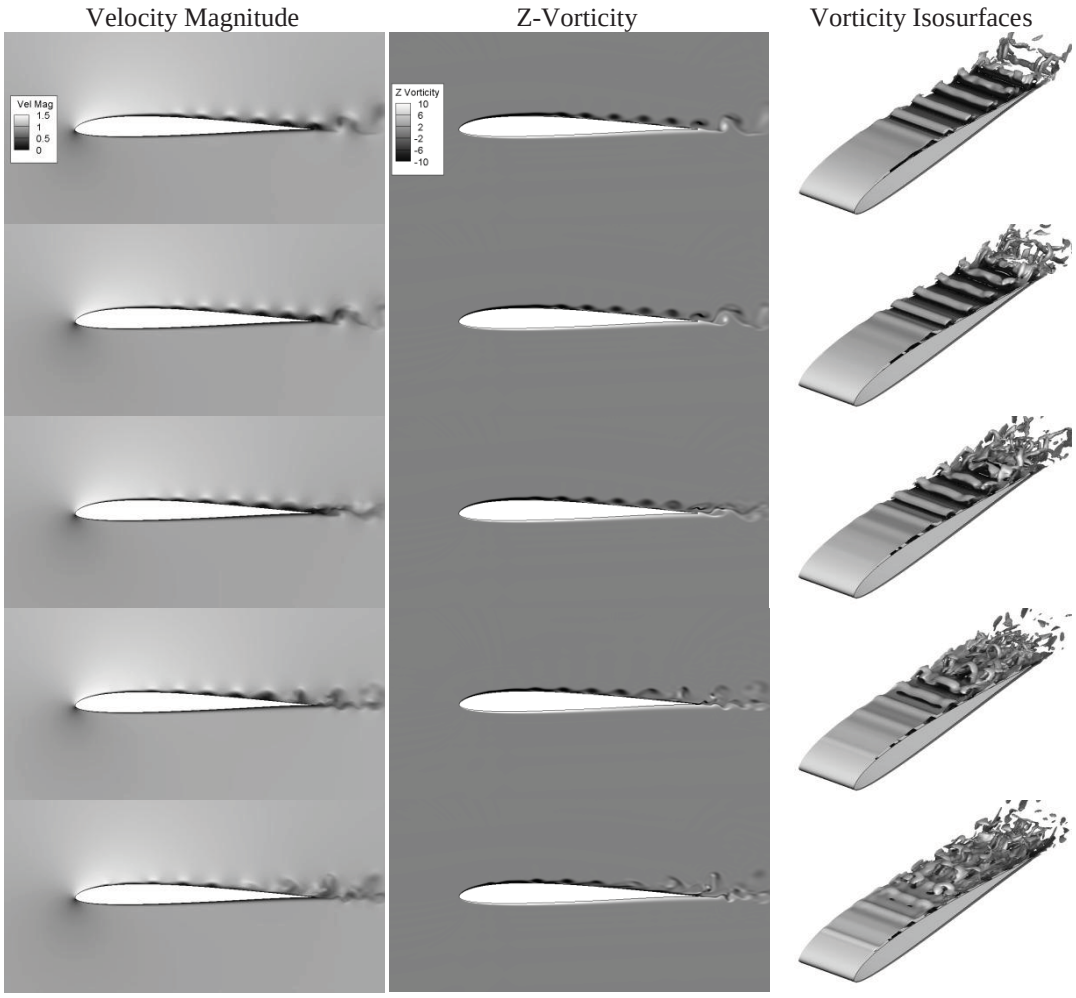

Figure 16. Instantaneous velocity magnitude, z-vorticity and vorticity isosurfaces for increasing values of D_c (D_c =4.9, 9.8, 19.7, 39.3 and 78.6) at τ=3.0.

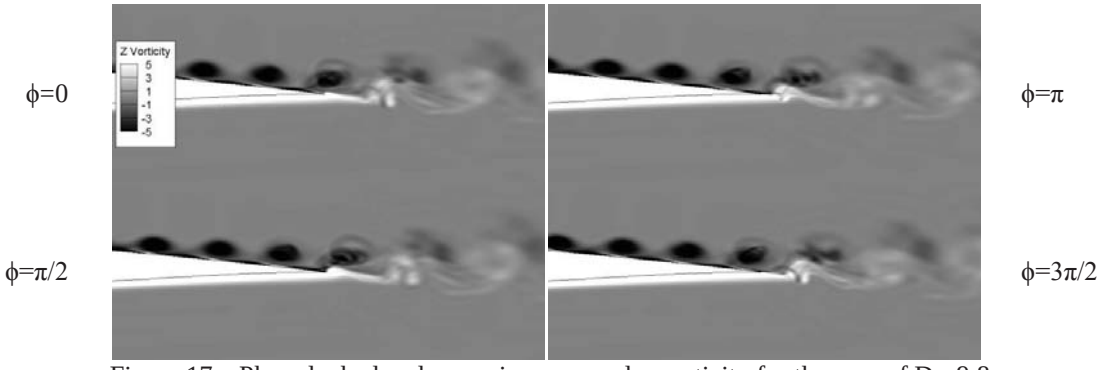

Figure 17 – Phase locked and spanwise averaged z-vorticity for the case of D_c=9.8

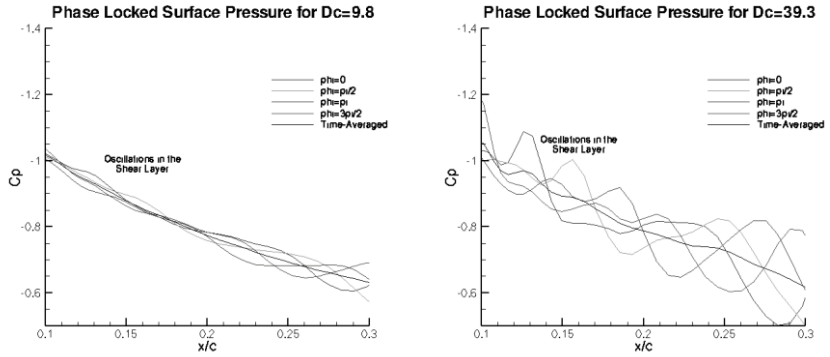

Figure 18. C_p around the actuator

V. Conclusions

The results of this study show that the low Reynolds number flow examined here can be reattached using plasma actuation as a disturbance force, even at very low levels of forcing. That the low levels of plasma actuation are still effective gives promise to further use of plasma actuation at higher Reynolds number, should the flow be able to be kept in the laminar/transitional regime.

Additionally, the transient effects associated with the initial response of the flow to the activation of plasma actuators and the unsteady, periodic effects seen once the flow reaches an equilibrium state show flow features not visible in the time averaged flow. These unsteady effects consist primarily of shed vortical structures either resulting from the breakdown of the separated shear layer or from the pulsed action of the plasma actuator. However, the examination of these unsteady effects provide a better understanding of the physical processes that promote the flow reattachment.

While the resulting flow does depend on the levels of plasma forcing, the response of the nondimensional forces shows itself to be nearly independent of the plasma forcing magnitude across the ranges tested in this study. The reattachment of the flow is dominated by the laminar separation bubble breaking down into a number of vortical structures, which then roll up onto each other and near trailing edge transition to create a large vortical structure. These larger structures cause a spike in the nondimensional forces. By τ=1.7, the flow can be considered reattached, though not quite at equilibrium.

Once the flow has reached equilibrium, a periodic nature has been shown to develop. For the scenarios tested, the shear layer near the leading edge is shown to regularly shed vortical structures which roll down stream, attached to the surface, until they lose coherence and transition to a more turbulent state. Should these structures maintain a level of coherence at the trailing edge, they will cause a higher level of oscillation in the nondimensional forces.

With the addition of the plasma actuation, the long term lift, drag, and moment are all shown to drop in magnitude. However, with this drop, the ratio of lift to drag is also shown to increase, providing an increased level of performance overall.

This work will continue to press forward to further understand the reattachment process involving laminar separation bubbles and how to mitigate the impulsive nature of the nondimensional forces associated with the reattachment process using various flow control strategies. Shear layer theory offers some interesting insight that may allows for more control over the initial, large vortex pairing event. Additionally, novel plasma actuator geometries, such as those developed by Roy and Wang [29], may be able to spread the impulsive nature over a longer time span.

Acknowledgments

This work was partially supported by AFOSR Grant FA9550-09-1-0372, monitored by Dr. Doug Smith. The first author would like to thank the University of Florida Graduate School Fellowship Award and the AFRL Summer Researcher Program for their financial support. The authors acknowledge the University of Florida High-Performance Computing Center for providing computational resources and support that have contributed to the research results reported within this paper.

References

[1] Bons, J.P., Reimann, D., and Bloxham, M., "Separated Flow Transitions on a LP Turbine Blade with Pulsed Flow Control," ASME Journal of Turbomachinery, Vol 130, No 2, April 2008.

[2] Gross, A. and Fasel, H.F. "Numerical Investigation of Low-Pressure Turbine Separation Control" AIAA paper 2008- 4321, June 2008.
[3] Amitay, M. and Glezer, A. "Controlled transients of flow reattachment over stalled airfoils," International Journal of Heat and Fluid Flow Vol. 23, pp. 690-699, 2002.
[4] Moreau, E. "Airflow control by non-thermal plasma actuators". Journal of Physics D: Applied Physics, Vol. 40, No 1, 2007
[5] Gaitonde, D.V., Visbal, M.R., and Roy, S. "A Coupled Approach for Plasma-Based Flow Control Simulations of Wing Sections," AIAA Paper 2006-1205, Jan 2006.
[6] Gaitonde, D.V., Visbal, M.R. and Roy, S. "Control of Flow Past a Wing Section with Plasma-based Body Forces," AIAA Paper 2005-5302, June 2005.
[7] Gaitonde, D.V., Visbal, M. R., and Roy, S. "Three-dimensional Plasma-Based Stall Control Simulations with Coupled First-Principals Approached," ASME Paper FEDSM2006-98553.
[8] Schatzman, D.M. and Thomas, F.O. "Turbulent Boundary Layer Separation Control with Plasma Actuators," AIAA Paper 2008-4199, June 2008.
[9] Greenblatt, D., Schule, C.Y., Romann, D., and Paschereit, C.O. "Dielectric Barrier Discharge Flow Control at Very Low Flight Reynolds Numbers," AIAA Journal Vol. 46, No. 6, June 2008.
[10] Roth, J.R., Sherman, D. M., and Wilkinson, S. P. "Boundary Layer Flow Control with a One Atmosphere Uniform Glow Discharge Surface Plasma," AIAA Paper 98-0328, Jan 1998.
[11] Gaitonde, D.V., Visbal, M.R., and Roy, S. "Control of Transitional and Turbulent Flows Using Plasma-Based Actuators," AIAA Paper 2006-3230, 2006.
[12] Patel, M.P., Ng, T.T., Vasudevan, S., Corke, T.C., and He, C. "Plasma Actuators for Hingeless Aerodynamic Control of an Unmanned Air Vehicle," AIAA Journal of Aircraft Vol. 44, No. 4, August 2007.
[13] He, C., Corke, T.C. and Patal, M.P. "Plasma Flaps and Slats: An Application of Weakly Ionized Plasma Acutators," AIAA Journal of Aircraft, Vol. 46, No. 3, Jun 2009.
[14] Rizzetta, D.P. and Visbal, M.R. "Plasma-Based Flow-Control Strategies for Transitional Highly Loaded Low-Pressure Turbines," ASME Journal of Fluids Engineering, Vol. 130, No. 4, April 2008.
[15] Huang, J., Corke, T. C. and Thomas, F. O., "Unsteady Plasma Actuators for Separation Control of Low Pressure Turbine Blades," AIAA Journal Vol 44, No. 7. 2006.
[16] Thomas, F.O., Kozlow, A. and Corke, T.C. "Plasma Actuators for Cylinder Flow Control and Noise Reduction," AIAA Journal Vol 46, No. 8, August 2008.
[17] Wang, C.C. and Roy, S. "Electrodynamic Enhancement of Film Cooling Of Turbine Blades," Journal of Applied Physics Vol. 104, Oct. 2008.
[18] Rizzetta, D.P. and Visbal, M.R. "Numerical Investigation of Plasma-Based Control for Low-Reynolds Number Airfoil Flows," AIAA paper 2010-4255.
[19] Greenblatt, D. and Wygnanski, I.J. "The control of flow separation by periodic excitation," Progress in Aerospace Sciences Vol. 36 pp. 487-545, 2000.
[20] Galbraith, M.C. and Visbal, M.R. "Implicit Large Eddy Simulation of Low-Reynolds-Number Transitional Flow Past the SD7003 Airfoil," AIAA paper 2010-4737. July, 2010.
[21] Rizzetta, D.P., Visbal, M.R., and Morgan, P.E. "A High-Order Compact Finite-Difference Scheme for Large-Eddy Simulation of Active Flow Control" AIAA Paper 2008-526, Jan. 2008.
[22] Beam, R.M. and Warming, R.F. "An Implicit Factored Scheme for the Compressible Navier-Stokes Equations," AIAA Journal Vol. 16, No. 4, April 1978.
[23] Shyy, W., Jayaraman, B. and Andersson, A., "Modeling of Glow Discharge-Induced Fluid Dynamics", Journal of Applied Physics, Vol. 92, No. 11, pp. 6434-6443, 2002.
[24] Visbal, M. R. and Gaitonde, D. V., "High-Order-Accurate Methods for Complex Unsteady Subsonic Flows," AIAA Journal, Vol 37, No.10, Oct 1999, pp 1231-1239
[25] Lele, C. A., "Compact Fine Difference Schemes with Spectral-Like Resolution," Journal of Computational Physics, Vol. 102, No. 1, 1992, pp. 16-42.
[26] Galbraith, M. C. and Visbal, M.R. "Implicit Large Eddy Simulation of Low Reynolds Number Flow Past the SD7003 Airfoil," AIAA paper 2008-225, Jan. 2008.
[27] Ol, M.V., McAuliffe, B.R., Hanff, E.S., Scholz, U, and Kahler, C. "Comparison of Laminar Separation Bubble Measurements on a Low Reynolds Number Airfoil in Three Facilities" AIAA Paper 2005-5149, June 2005.
[28] Bons, J.B., Solndergaard, R., and Rivir, R.B., "Turbine Separation Control Using Pulsed Vortex Generator Jets," ASME Journal of Turbomachinery, Vol. 123, No. 2, 2001.
[29] Roy, S. and Wang, C.C. "Bulk flow modification with horseshoe and serpentine plasma actuators," Journal of Physics D: Applied Physics, Dec. 2008.